Revista Mexicana de Astronomía y Astrofísica, **40**, 81–98 (2004)

NUMERICAL WIND MODELING FOR THE SAN PEDRO MÁRTIR SIERRA IN BAJA CALIFORNIA

K. Vogiatzis

National Optical Astronomy Observatory, Tucson, AZ, USA

and

D. Hiriart

Instituto de Astronomía
Universidad Nacional Autónoma de México, Ensenada, B. C., México

Received 2004 February 10; accepted 2004 March 11

RESUMEN

Presentamos la simulación numérica del viento en la Sierra de San Pedro Mártir para realizar una evaluación preliminar de los posibles sitios donde instalar nuevos telescopios. Como criterio inicial, se eligieron los puntos más altos de la sierra, pero a la vez de fácil acceso. Se presentan la altura de la capa límite y el efecto de la turbulencia en los diferentes sitios para velocidades y direcciones del viento típicas.

ABSTRACT

We have used numerical simulations of wind over San Pedro Mártir Sierra to make a first evaluation of potential sites for astronomical use. Initially, we have analyzed the highest points on the Sierra but with easy access. We present the turbulence and size of the boundary layer for typical speed and wind directions on these sites.

Key Words: **ATMOSPHERIC EFFECTS — SITE SELECTION — TURBULENCE**

1. INTRODUCTION

Recently, San Pedro Mártir Sierra has been considered by several astronomical groups as a potential site to install large diameter telescopes. This is mainly due to the large number of cloudless nights during the year and the reasonably low amount of water vapor (Erasmus & van Staden 2002).

To take advantage of their potential high angular resolution, the new telescopes will rely critically on adaptive optics to correct the atmospheric disturbance. Therefore, atmospheric turbulence for the candidate sites has to be studied. Night-time seeing measurements made at the San Pedro Mártir National Observatory (SPM-NO) show excellent mean values (Echevarría et al. 1998; Michel et al. 2003). Since the seeing is strongly affected by the atmospheric turbulence produced by the local topography, it seems possible to find places on the San Pedro Mártir Sierra that may have similar or even better seeing values than the site of SPM-NO.

Instead of deploying seeing measuring instruments on all the highest points of the Sierra, the list of candidate sites may be narrowed by a preliminary evaluation using Computational Fluid Dynamics (CFD). This technique provides detailed airflow information over an arbitrary chosen variety of initial and boundary conditions in the applicable Reynolds number ranges, and the calculations can be performed relatively quickly and at minimal cost. The earliest applications of CFD to site characterization involved ground layer turbulence investigation above the Gemini site on Mauna Kea and Cerro Pachón (De Young & Charles 1995). Advances in computational power allowed in recent years a more elaborate use of CFD on the mesoscale level (Masciadri 2003; Riemer & Zängl 2002).

This paper presents the results of CFD modeling of wind flow above several candidate sites on San Pedro Mártir Sierra, with emphasis on the topographically induced turbulence.

The goal of this study is to investigate the behavior of wind flow above the high altitude sites on San Pedro Mártir Sierra and to gain insight into possible peculiarities they may exhibit. It also provides an overview of the kind of analysis tools that may be helpful to the community engaged in site characterization and selection procedures for large telescopes.

In § 2 of this paper we present the candidate sites and the rationale for their selection. The method of calculation and cases of study are shown in § 3. The results and their discussion are presented in § 4 and § 5, respectively. Finally, the conclusions are presented in § 6.

2. THE SITES

Five of the highest points of the Sierra were selected. They were chosen on the basis of ease of access and low impact on the construction costs. This places were: San Pedro Mártir National Observatory, Alamillos de Arriba, Venado Blanco, Botella Azul, and La Corona.

San Pedro Mártir National Observatory. The site of SPM National Observatory is the best characterized site for astronomical purpose in the whole Sierra. Weather conditions for San Pedro Mártir have been reported (Tapia 1997; Walker 1984; Alvarez 1982; Alvarez & Maisterrena 1977; Mendoza, Luna, & Gómez 1972; Mendoza 1971, 1973; Michel et al. 2001). Measurements of seeing conditions have been done for this site (Michel et al. 2003; Conan et al. 2002; Echevarría et al. 1998; Avila, Vernin, & Cuevas 1998). Sky emission at 10 μm has been reported by Westphal (1974). Wind spectrum at the site has been measured by Hiriart, Ochoa, & García (2001). Opacity of the sky at millimetric wavelengths has been discussed by Hiriart (2003a,b) and Hiriart et al. (1997). A summary of the results of these and other studies has been compiled by Avila, Cruz–González, & Tapia (2003).

Alamillos de Arriba. This is a plateau right in front of the Observatory site. It has the advantage of having a big flat area for construction and, due to its proximity, it offers the possibility to share the facilities of the Observatory.

Venado Blanco. It is a peak to the N–NW of San Pedro Mártir Observatory and may be an interesting site to install a telescope. There is a bumpy road to the base of the peak, but no electric power or other facilities are available at the site.

Botella Azul. This place is located at 10 km of the Observatory in the southeast direction. It is very near to the Picacho del Diablo. This site was considered as a potential site to install the Large Millimeter Telescope (LMT). As part of the site survey for the LMT, a radiometer at 210 GHz to monitor the sky opacity was installed there from 1995 to 1997 (Hiriart 2003b). Also, a meteorological station was installed there but never got reliable measurements. The site can only be accessed by hiking. One of the drawbacks of this site is that Picacho del Diablo lies in front, and it may produce some interfering wakes when the wind blows from the east.

La Corona. La Corona is located at the west side of the Sierra. This place was a candidate site for the 2 m telescope now installed in the Mexican state of Sonora and operated by the Instituto Nacional de Astrofísica, Óptica y Electrónica (INAOE). It is believed that this site may have a better seeing than the one at the Observatory because the wind upstream may be less turbulent. This site is the westernmost site at the sierra plateau and it may be interesting to compare it to the eastern ridge results.

Figure 1[1] presents the Digital Elevation Map (DEM) of the available topographical data. The range and the usable size of this rectangle is 80×220 km and is centered at (640,000:3,430,000)(UTMx:UTMy). The horizontal resolution is 200 m. Although maps with higher resolution are available, we used this DEM for a first try and selection of the sites. The San Pedro Mártir Sierra has a smooth, gently ascending terrain from the west side, but abruptly descending terrain to the east. The National Astrononomical Observatory, operated by the National Autonomous University of México through the Institute of Astronomy, is located at the east ridge of the Sierra.

Table 1 lists the candidate sites on San Pedro Mártir Sierra. The table shows their names, approximate geodetic location, Universal Transverse Mercator (UTM), and their elevation accurate to 1 meter.

For the calculations, we selected a smaller DEM of about 35×30 km since all the sites considered are in close proximity. This allows us to evaluate the interactions of the airflow on a large scale. The terrain details for the processed DEM can be seen in Figure 2. The sites of interest from Table 1 are identified. For reference we have included the highest point in the sierra, Picacho del Diablo, located a the bottom right of the figure and identified by the number 6. Picacho del Diablo has an elevation of 3001 m and is located at latitude 30° 59′ 30″ N and longitude 115° 22′ 34″ W.

3. METHOD OF CALCULATION

The calculations were fully three-dimensional, and the flow was assumed to be steady, incompress-

[1] To see all figures in color, please refer to the electronic version of this paper.

TABLE 1

CANDIDATE SITES ON SAN PEDRO MÁRTIR SIERRA FOR ASTRONOMICAL USE

Site	Name	Lat. [N]	Long. [N]	UTMx	UTMy	Elev. [m]
1	SPM National Observatory	31° 02′ 41.8″	115 ° 27′ 46.6″	646692	3435573	2800
2	Alamillos de Arriba	31° 01′ 38.9″	115 ° 26′ 55.7″	648071	3433652	2766
3	Venado Blanco	31° 05′ 20.7″	115 ° 29′ 07.6″	644478	3440439	2761
4	Botella Azul	30° 58′ 15.0″	115 ° 23′ 43.8″	653252	3427474	2910
5	La Corona	31° 00′ 08.9″	115 ° 33′ 43.3″	637289	3430735	2604

ible and isothermal. The effects of turbulence were modeled through the use of the k-ϵ approximation (De Young & Charles 1995) modified to account for high Reynolds number effects. Here k is the turbulent kinetic energy per unit mass and ϵ is the turbulent energy dissipation rate per unit mass. The commercial software STAR-CD was used to solve the Reynolds-averaged form of the Navier-Stokes conservation equations of mass and momentum.

The first step in performing numerical simulations is always grid generation. The terrain has to be modeled as part of the grid boundary. Although the software used is capable of solving arbitrary grids, performance can be improved if a uniform grid is used in both directions. Sometimes, topographic data of the sites are not readily available in a uniform rectilinear form, so additional commercial software and in-house-developed code had to be used to convert the data. The DEMs were translated to ASCII triads (X,Y,Z) with fixed horizontal spatial resolution, which became the rectangular basis of the grid. The X and Y values are UTM coordinates (m) while Z is the elevation (m). To generate the third dimension of the grid a given number of points were placed between the local surface elevation and the chosen fixed ceiling elevation. The vertical distance between two consecutive nodes was chosen to be a term of a geometric series with a ratio of 1.2. As a result, a vertical spatial resolution of approximately 1 m was achieved close to the ground, where high velocity gradients exist. Close to the ceiling where the airflow is expected to be more uniform, the resolution can be as coarse as a few hundred of meters. The vertical resolution of a representative grid is shown in Figure 3.

For improved accuracy and in order to facilitate proper application of boundary conditions the resulting computational box orientation was chosen so that a face was always normal to the applied wind direction, as is shown in Figure 4. The inlet wind velocity profile used is generally given by

$$u(z) = U \left(\frac{z - z_0}{h} \right)^{0.6} . \tag{1}$$

The value of z_0 is dictated by the local surface elevation at the inlet, while U and h are chosen to yield the reported wind speeds at high altitude where the pressure level is 470 mb. It is important to note that this profile is more realistic than a uniform wind speed level, and also more correct than the traditional 1/7 power law for flat plate turbulent boundary layer. Atmospheric boundary layer measurements (Davenport 1960) indicated that over rough terrain the exponent for a stable layer, such as a nocturnal one, could be as high as 0.6, rather than 0.15-0.2, which is often recorded during the day. The inlet air properties were taken to be those of the atmosphere at the average elevation of the computational domain. The inlet air was given a turbulent intensity $I = u'/U$ of 2–5 % (see § 4) that is, the rms value of the fluctuating part of the velocity u' was 2.5–5 % of the local (free stream) velocity value U. The other parameter of the turbulence model, the rate of turbulent energy dissipation ϵ, was calculated from the turbulent kinetic energy k, by assuming a mixing length L of 5 m and equilibrium between turbulent energy production and dissipation.

On the topographic surface a no-slip boundary condition was placed with prescribed roughness height, depending on the terrain type (Wieringa 1996). For most of the sites an equivalent surface roughness height of 0.01 m is representative of barren land. In the case of San Pedro Mártir Sierra the surface was raised to 0.05 m, typical of wooded areas. The sides and ceiling of the domain were given free-slip boundaries with zero normal velocity component; the outflow boundary condition set all normal derivatives to zero.

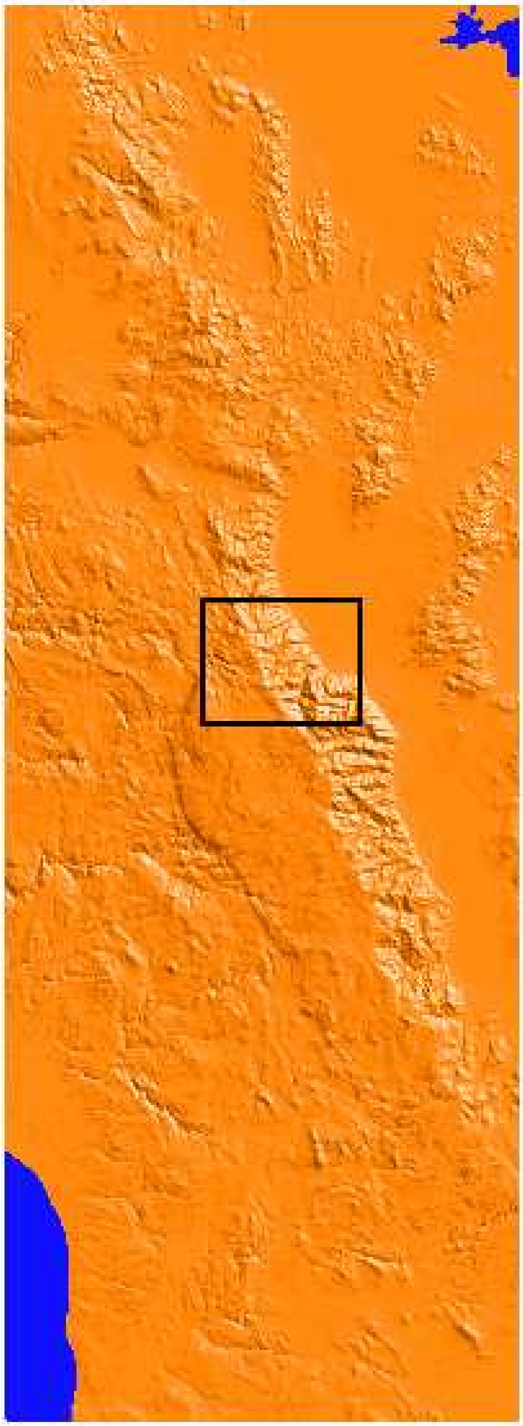

Fig. 1. Digital Elevation Map of the Baja California Peninsula. North is at the top and east to the right. This map covers from 30° to 32° in latitude, and from 115° to 116° W in longitude. The rectangle shows the area used in the simulations.

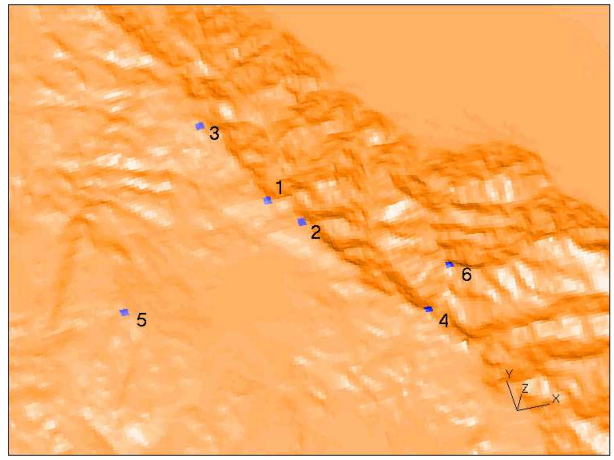

Fig. 2. Digital Elevation Map close-up showing the location of the sites of interest (see Table 1). This subset of the original DEM was used in the simulations. The highest point in the Sierra, Picacho del Diablo (6) is shown for reference. North is to the top and east to the right.

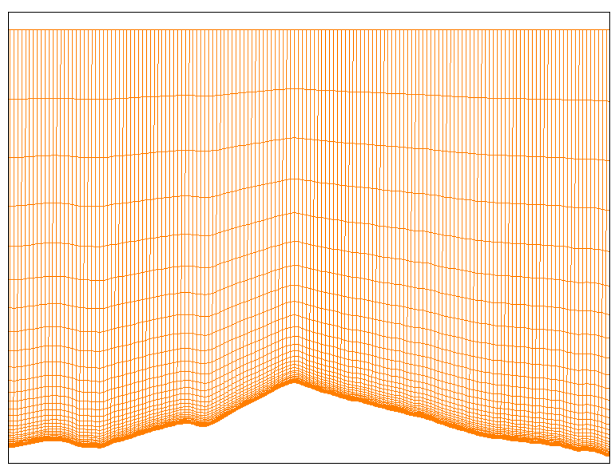

Fig. 3. Vertical cross-section of a representative grid.

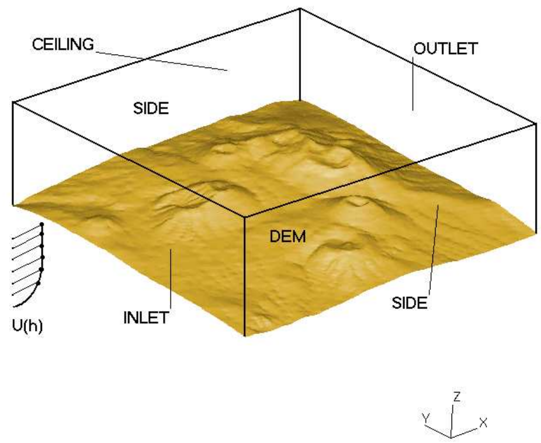

Fig. 4. Representative set-up configuration for the computational domain.

3.1. *Simulated Cases*

Echeverría et al. (1998) have presented measurements of wind velocity for 386 nights in SPM Observatory. They found, as a general trend, that wind speed seldom exceeds the 11 m/s; the predominant and strongest wind comes from the S–SW; the wind rarely comes from the E and W–NW, and the speed of the wind is almost uniform. They show the wind roses for the site separated every three months: January–March (winter), April–June (spring); July–September (summer) and; October–December (autumn). The spring distribution is uniform, while the summer distribution shows a gap in the west direction. During the summer, winds appear to come more uniformly from the east, with very few W–NW winds. Wind speeds during summer and spring are almost constant at 5.5 m/s. Winter and autumn wind distributions are bipolar, with a rotation of about 90° orientation with respect to each other. During the winter, predominant winds come from the NE and SW, while in the autumn the predominant winds come from NW and SE. The speed distribution during autumn has a more or least uniform value of 5.5 m/s, while the winter distribution has roughly the same mean value, but higher wind dispersions due to the higher speed for winds coming from the N. The wind directions prevailing in their plots were used in the simulations presented in this study.

Table 2 lists the various cases simulated. The cases have been given a code name B1 to B8 for easy referencing. The name of the case and the upwind direction are shown in Column 1. The size of computational domain is shown in Column 2 and the total number of cells in Column 3. The corresponding horizontal resolution was 200 meters with a fixed ceiling of 10,000 m. The primary direction (Column 6) follows the trend of the wind shown by the wind rose data of Echeverria et al. (1998) as they defined the seasons. North is 0° and east 90°. The High Altitude Velocity (Column 5) is the average velocity at 200 mb (12 km over the sea level), as reported by Carrasco & Sarazin (2003), for the three months that define the season.

4. RESULTS

The results of the instantaneous velocity field,u, can be separated into a mean part, U, plus a fluctuating part with zero mean u', ($u = U + u'$). The thickness of the boundary layers and the size of wakes are characterized by the level of appreciable turbulent kinetic energy $k = \frac{1}{2}(\langle u'^2 \rangle)$. Outside those regions it assumes its regular values for free atmospheric turbulence (not associated with shear layers and jet stream), namely 2.5–5.0 % intensity. A more obvious variable to monitor would be the root-mean-square value of u', since it is given in m/s and can be directly measured. In this case the limit value could be set at 0.3 m/s, which is 2.5–5 % or less of the mean free stream velocity value outside a given boundary layer considered here. The rms of the fluctuating part of the wind velocity is given by $u'_{rms} = \alpha\sqrt{k}$. Depending on the type of flow the factor α takes values between 0.8 and 1.2.

4.1. *Wind Velocity Field*

Figures 5 to 14 are a graphical representation of the results for the wind velocity field at a given site. They consist of two type of plots, arranged side by side. On the left, contour plots of u'_{rms} calculated with a factor of $\alpha = 1$ are shown. The color scale ranges from 0.3 m/s to 1.7 m/s, which translates to turbulent intensities I of 2.5–5 % for the low limit and 15–25% for the high limit, depending on the free stream velocity levels. The estimated boundary layer thickness assumes an end of the effective boundary layer at I= 5 %. On the right, countour plots of $\|\vec{U}\|$ are shown. The color scale ranges from 0 to 14 m/s. Overlaid vectors show the local direction of flow. The plots are made in vertical planes passing through the summit of interest, and the viewing angle is perpendicular to the wind and such that the direction of the flow is from right to left.

4.2. *Boundary Layer*

Table 3 summarizes the boundary layer thickness, in meters, estimated from the calculations. Eight cases were simulated for the San Pedro Mártir

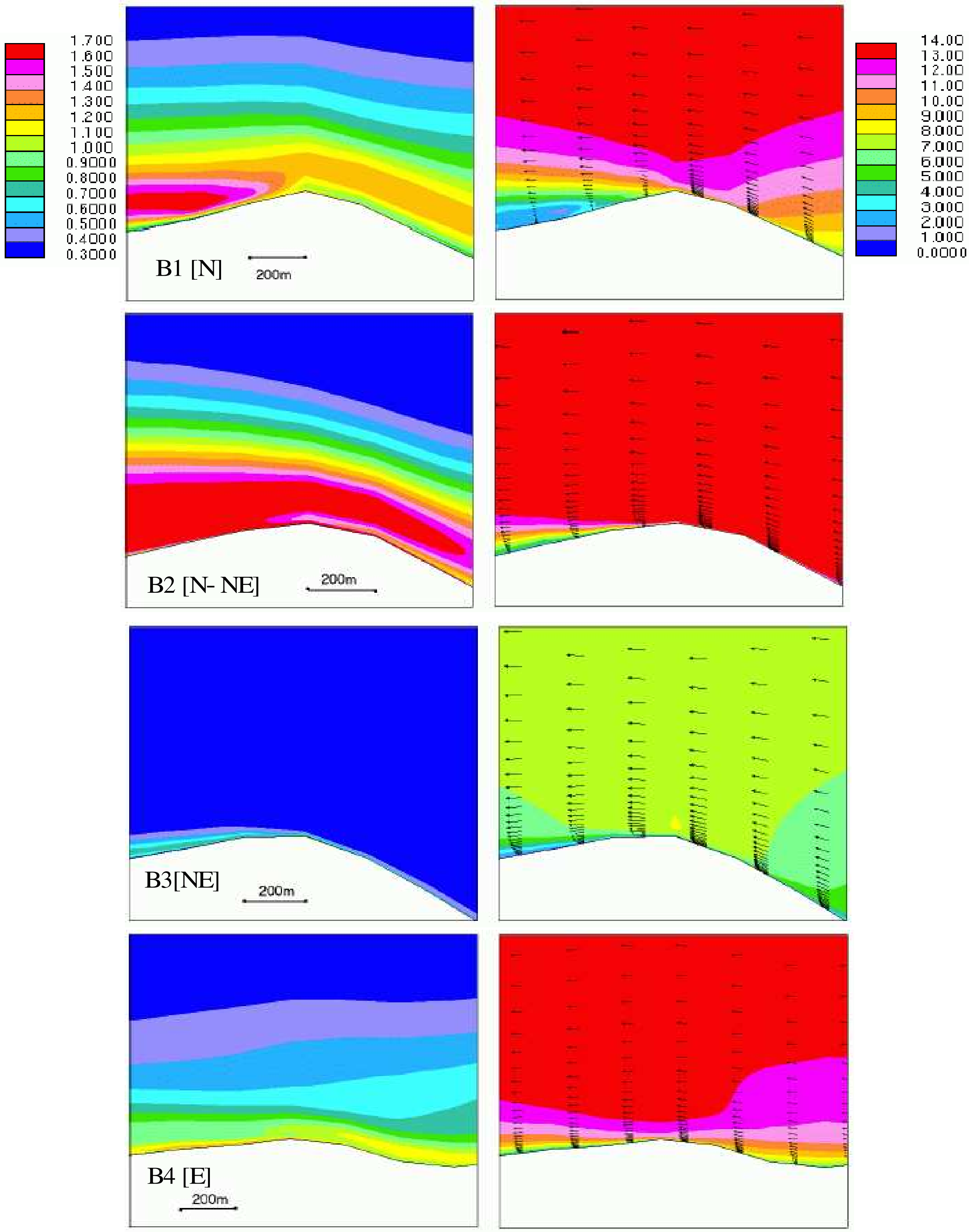

Fig. 5. RMS velocity contours (*left*) and mean velocity magnitude contour/vector plot (*right*) for cases **B1** to **B4** for **San Pedro Mártir Observatory**. Color scales for the plots are in m/s.

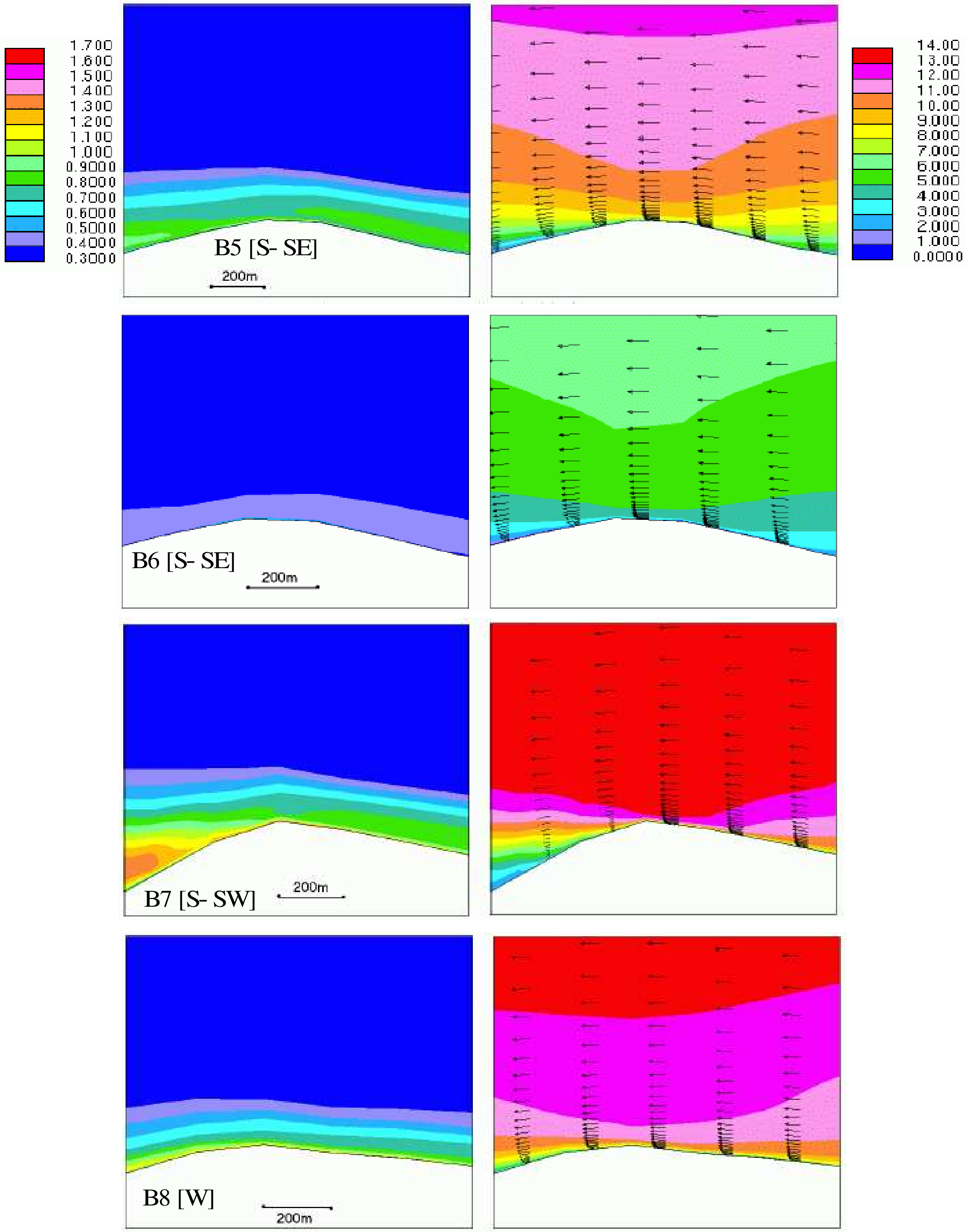

Fig. 6. RMS velocity contours (*left*) and mean velocity magnitude contour/vector plot (*right*) for cases **B5** to **B8** for **San Pedro Mártir Observatory**. Color scales for the plots are in m/s.

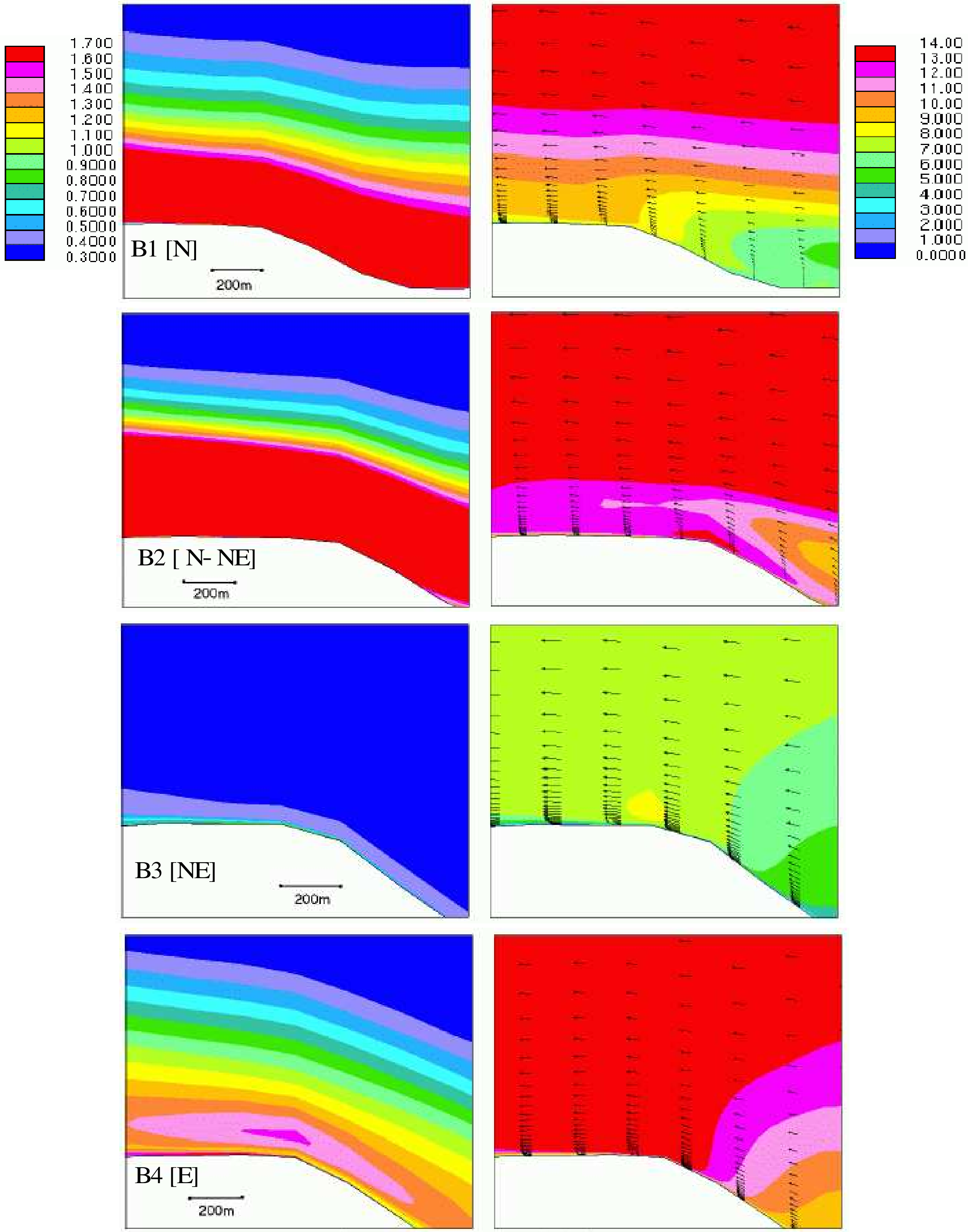

Fig. 7. RMS velocity contours (*left*) and mean velocity magnitude contour/vector plot (*right*) for cases **B1** to **B4** for **Alamillos de Arriba**. Color scales for the plots are in m/s.

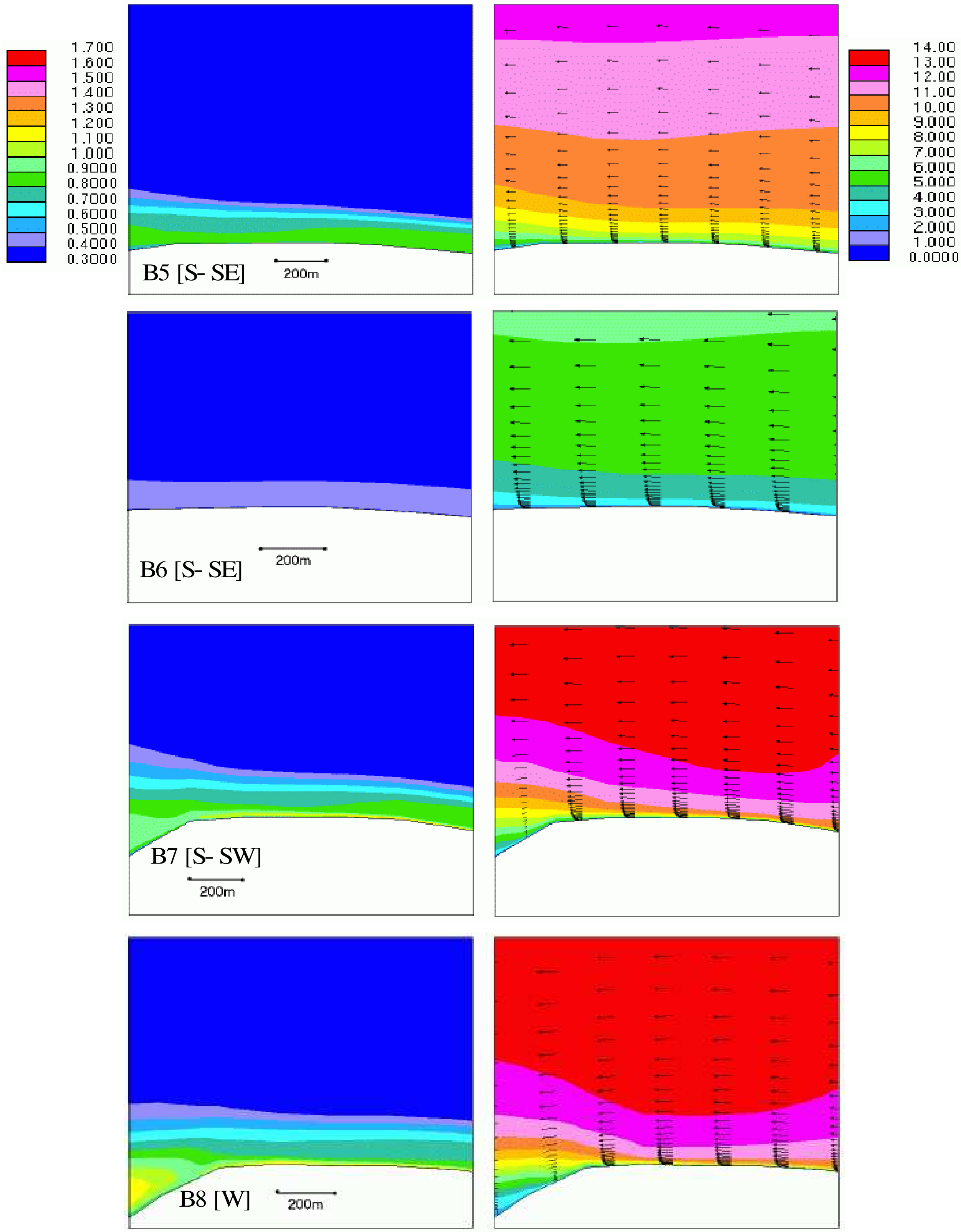

Fig. 8. RMS velocity contours (*left*) and mean velocity magnitude contour/vector plot (*right*) for cases **B5** to **B8** for **Alamillos de Arriba**. Color scales for the plots are in m/s.

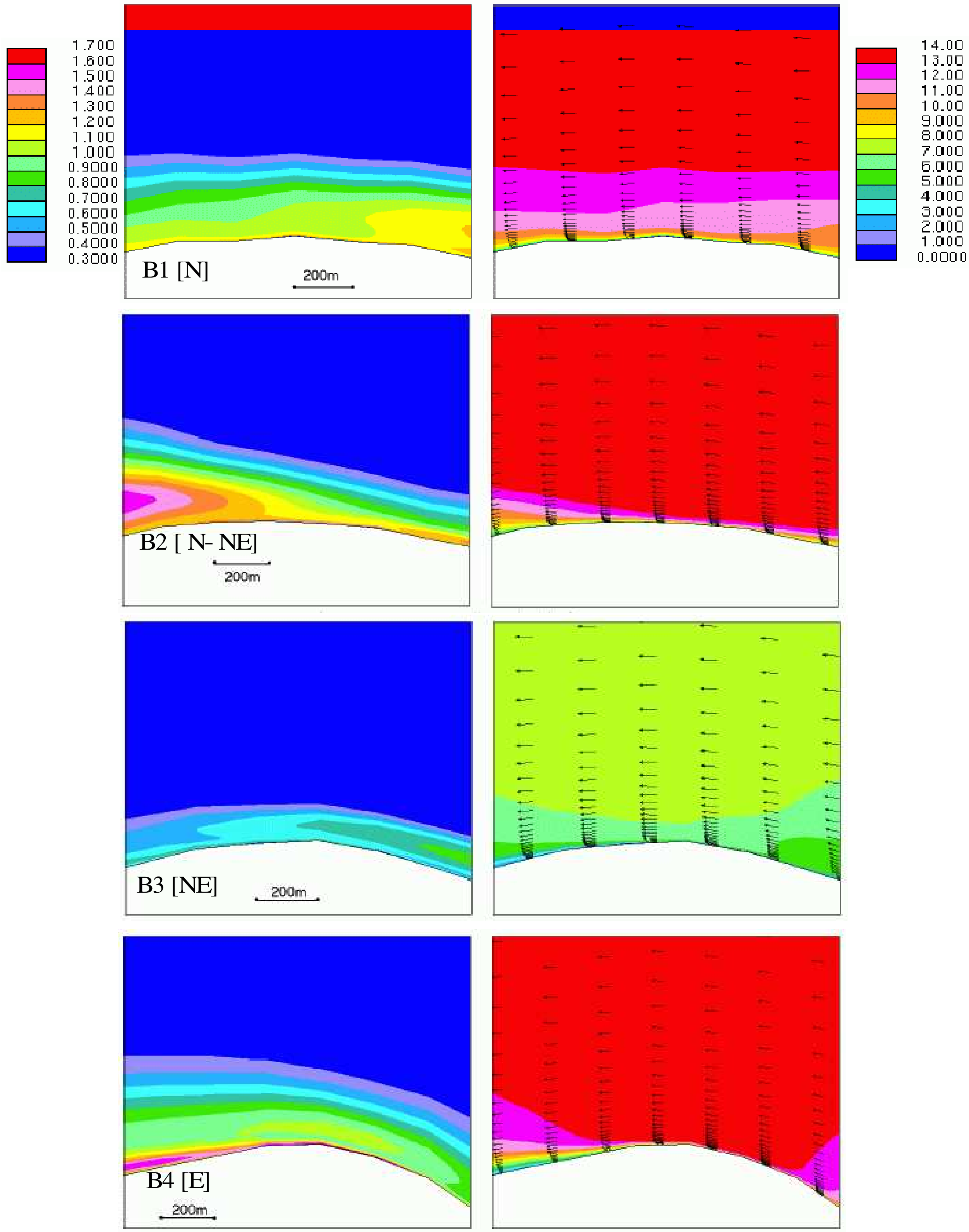

Fig. 9. RMS velocity contours (*left*) and mean velocity magnitude contour/vector plot (*right*) for cases **B1** to **B4** for **Venado Blanco**. Color scales for the plots are in m/s.

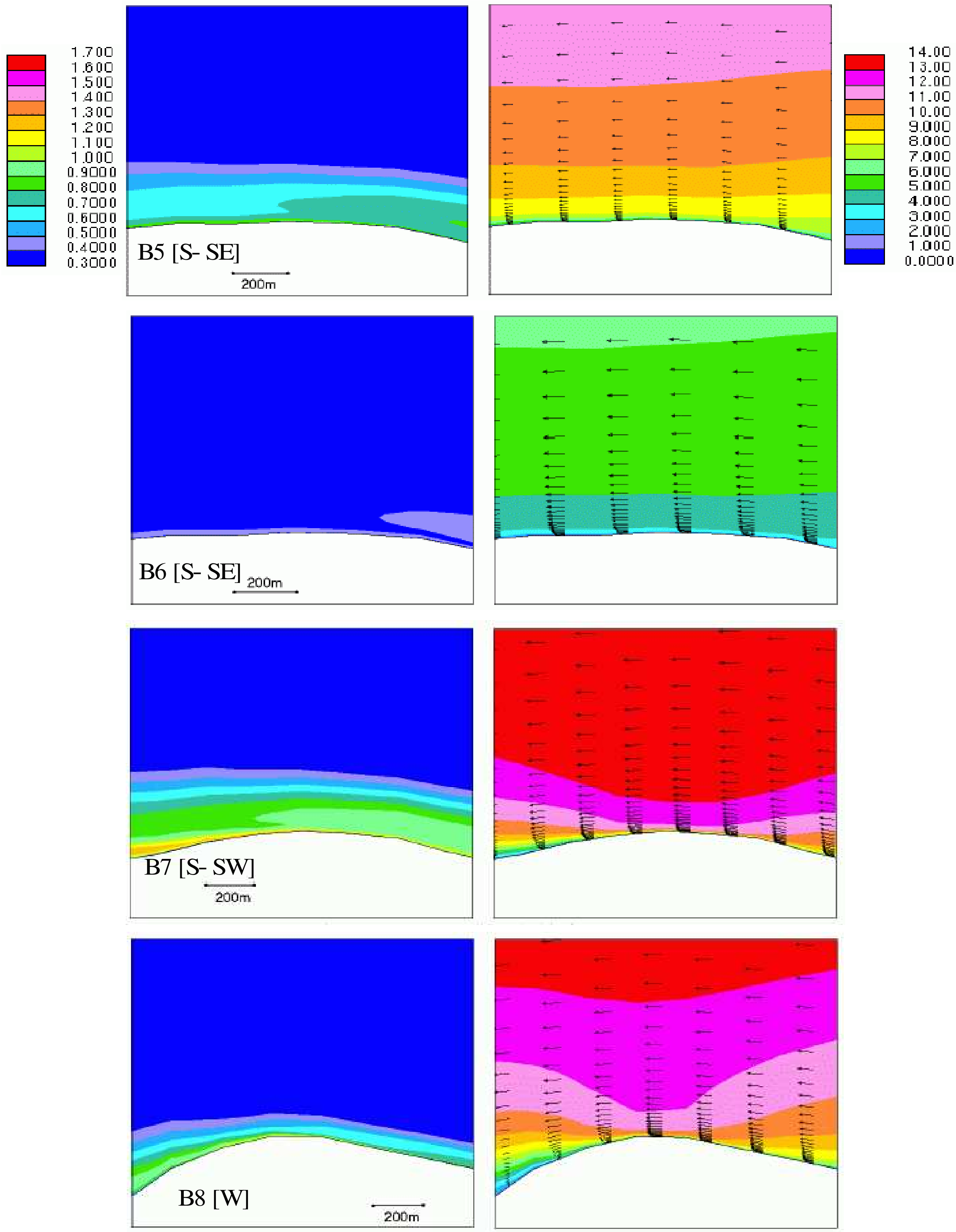

Fig. 10. RMS velocity contours (*left*) and mean velocity magnitude contour/vector plot (*right*) for cases **B5** to **B8** for **Venado Blanco**. Color scales for the plots are in m/s.

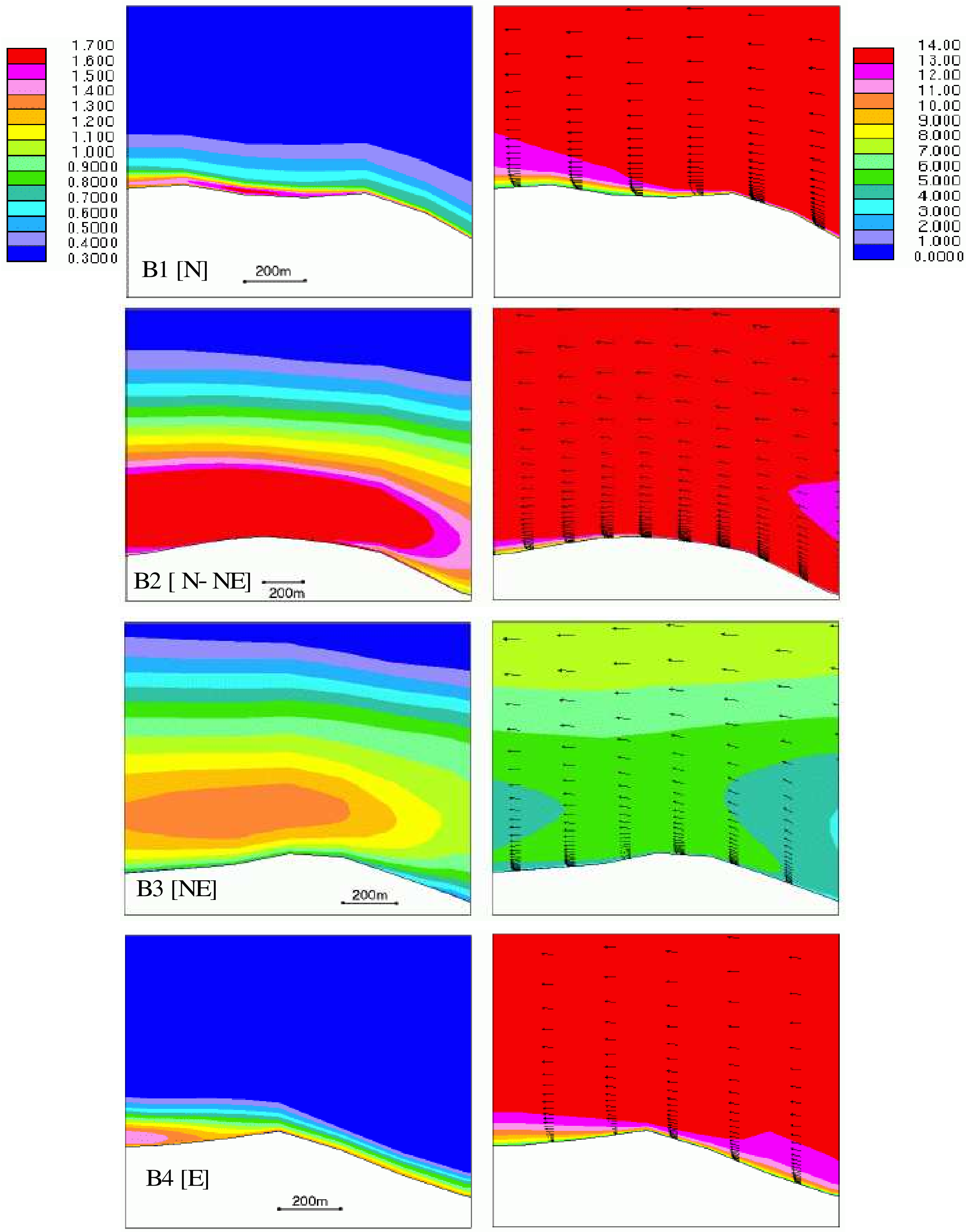

Fig. 11. RMS velocity contours (*left*) and mean velocity magnitude contour/vector plot (*right*) for cases **B1** to **B4** for **Botella Azul**. Color scales for the plots are in m/s.

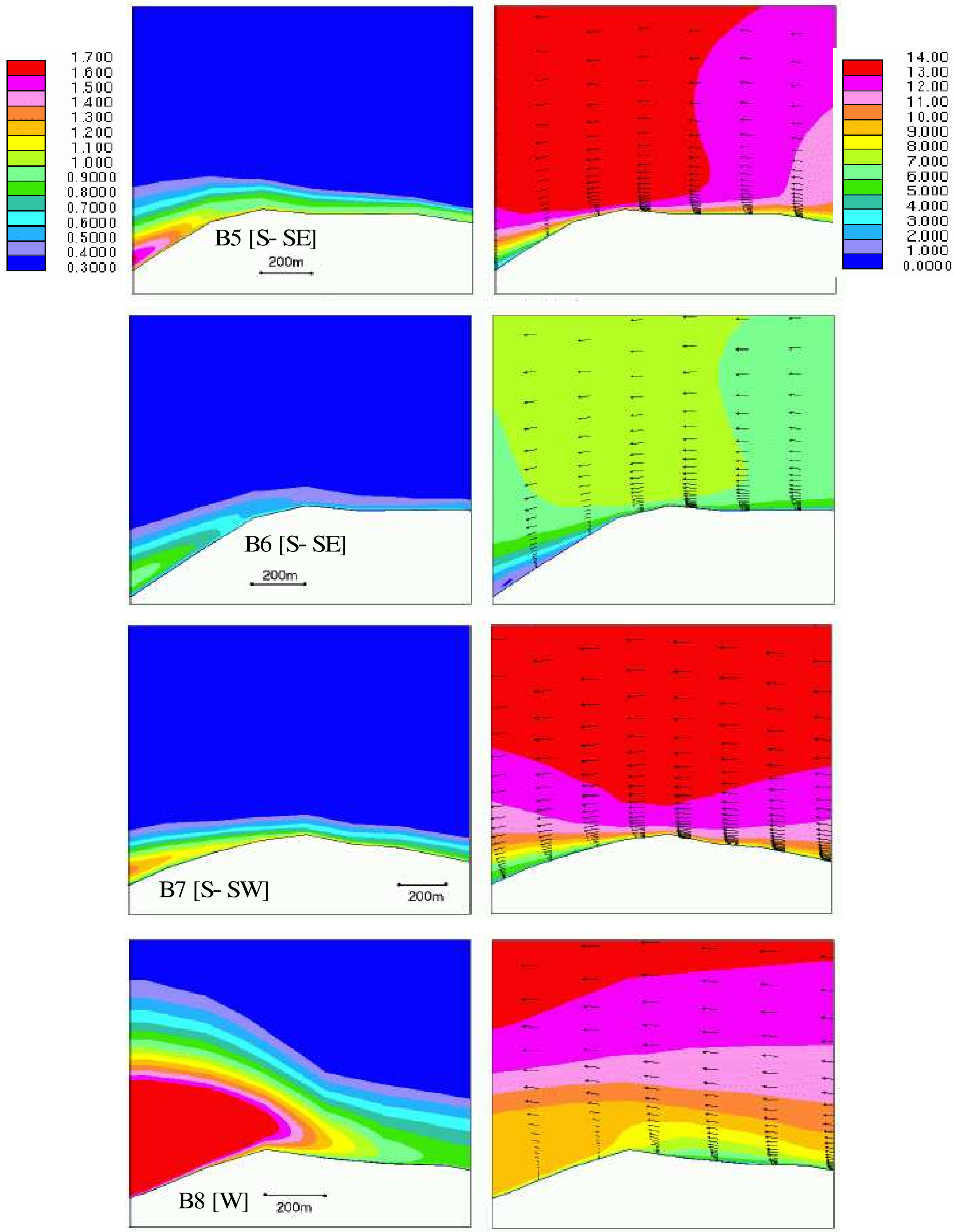

Fig. 12. RMS velocity contours (*left*) and mean velocity magnitude contour/vector plot (*right*) for cases **B5** to **B8** for **Botella Azul**. Color scales for the plots are in m/s.

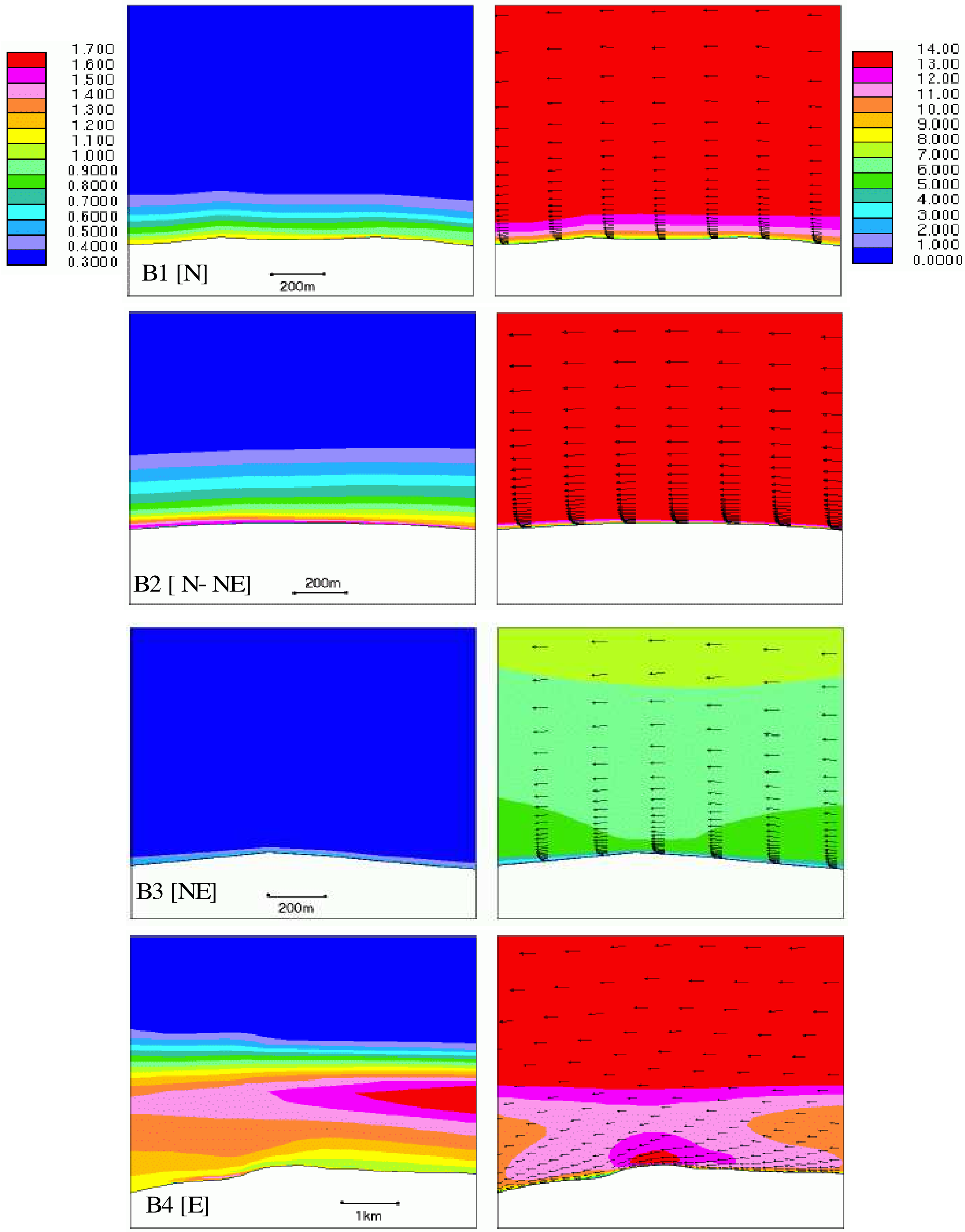

Fig. 13. RMS velocity contours (*left*) and mean velocity magnitude contour/vector plot (*right*) for cases **B1** to **B4** for **La Corona**. Color scales for the plots are in m/s.

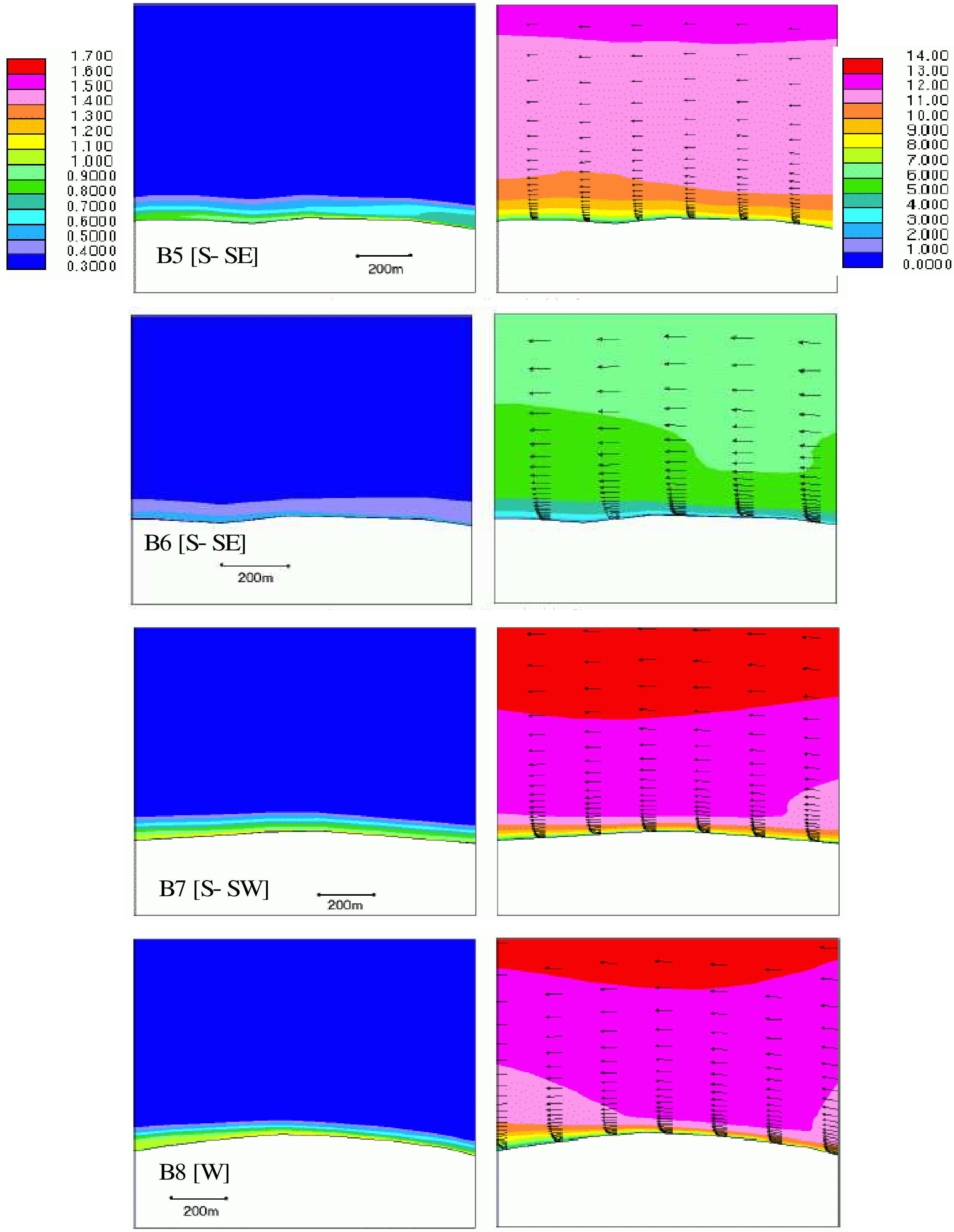

Fig. 14. RMS velocity contours (*left*) and mean velocity magnitude contour/vector plot (*right*) for cases **B5** to **B8** for **La Corona**. Color scales for the plots are in m/s.

TABLE 2

STUDY CASES FOR SAN PEDRO MÁRTIR SIERRA.

Case	Size [km]	Cells	Season	Wind Speed [m/s]	Wind Az. [°]
B1 [N]	35×30	1050000	Autumn	30.2	000
B2 [N–NE]	30×30	900000	Winter	36.8	015
B3 [NE]	30×30	900000	Summer	14.3	045
B4 [E]	35×30	1050000	Spring	26.8	090
B5 [S-SE]	25×30	750000	Spring	26.8	170
B6 [S-SE]	25×30	750000	Summer	14.3	170
B7 [S-SW]	30×35	1050000	Autumn/Winter	33.5	210
B8 [W]	35×30	1050000	Autumn	30.2	270

area, where the five locations of interest shown in Table 1 are considered. The bottom row (rightmost column) in the table shows the mean value of the boundary layer thickness for each case (site). The dashed line for the two case in B6 means that the boundary layer thickness is less than 5 m. A complete list of the wind input velocities used in the eight cases of study, B1 to B8, is shown in Table 2. Cases B5 and B6 differ only in the mean velocity of the input profile.

5. DISCUSSION

San Pedro Mártir Observatory. The thicker and more turbulent layer at this site occurs when the wind blows from the North; i.e., when the wind blows along the sierra ridge. The lowest values of the boundary layer thickness, cases B3 and B6, correspond to typical wind conditions during summer. This season has been reported as the one with the lowest mean values of measured seeing (Michel et al. 2003; Echeverría et al. 1998).

Alamillos de Arriba. Even though this site is close to the SPM-NO site, the boundary layer thickness behaves very differently, specially when the wind blows from the N-NE and E. This may be due to the effect of the wind passing over a slightly higher ridge toward those directions as seen from this site.

Venado Blanco. In this peak the boundary layer has a similar behavior to that of the SPM-NO site. When compared to SPM-NO site, it has thiner boundary layers for wind blowing from the west, but somewhat thicker for the predominant winds from the S-SW.

La Corona. This place presents the lowest boundary layer in most of the studied cases, including for winds predominant from the S-SW. The extremely large boundary layer from wind blowing from the east, case B4, is due to the presence of Picacho del Diablo in that direction. The effect of the wake produced by Picacho is also enhanced by the lower elevation of La Corona.

The Corona being the first high point reached by the upwind from the seashore, it benefits from the cold ocean currents that reduce the height of the inversion layers, and from the laminar air flow set up over the ocean (Walker 1971), although these may produce higher values of humidity at the site.

Botella Azul. The thicker boundary layer of this site occurs during the winter, when winds blow preferentially from the N–NE; i.e., the direction of Picacho del Diablo. Because both sites have the same elevation, the effect of the wake produced by Picacho is not as disrupting as in the case of La Corona. Curiously, after La Corona, this is the site with the thinnest boundary layer for the prominent and dominant winds. On the other hand, Botella Azul has almost the same amount of precipitable water vapor as the SPM-NO site (Hiriart 2003b).

6. CONCLUSIONS

1. From the previous discussion and according to the results of the simulations for the cases of study, La Corona showed to be the best site, with potentially good sky quality due to its low layer wind turbulence. Because winds from the E are very rare, wakes from the Picacho del Diablo may be unimportant.

2. Since Venado Blanco has a behavior of the boundary layer similar to that of San Pedro Mártir for most of the wind directions, this may be a site with similar or slightly better seeing conditions than the Observatory site.

TABLE 3

BOUNDARY LAYER THICKNESS (m) FOR SAN PEDRO MÁRTIR SIERRA.

Name	B1 [N]	B2 [N–NE]	B3 [NE]	B4 [E]	B5 [S–SE]	B6 [S–SE]	B7 [S–SW]	B8 [W]	MEAN
San Pedro Mártir	400	350	20	300	150	10	150	100	185
Alamillos de Arriba	600	600	20	600	120	..	150	120	276
Venado Blanco	220	200	100	220	150	..	200	50	145
Botella Azul	100	800	700	100	80	20	50	350	263
La Corona	100	200	10	2000	100	20	40	40	72
MEAN	284	430	170	305	120	11	118	132	...

3. Seeing measurements at San Pedro Mártir by Echeverría et al. (1998) are consistent with some of our results. In particular, measured seeing values are worst when the wind blows from the North in winter. It should be kept in mind that turbulence layer thickness depends not only on direction but also on speed.

4. The next steps in site simulations include enhancements in the spatial resolution as well as the inclusion of thermal effects, once information on temperature profiles upwind of the sites of interest becomes available. Thus, it will be possible to assess the quality of a site more directly.

5. CFD simulations of wind flow above candidate sites can provide mean and rms velocity fields, as well as vorticity, so as to calculate the intensity and measure the thickness of boundary layers and the length of wakes. They can also produce temperature fields and density gradients in order to characterize the thermal boundary layer of a potential site. The combined effect of mechanical and thermal turbulence is one of the key criteria in a site characterization procedure, and CFD can help towards an optimum selection.

6. Verification of the CFD results is also needed, especially in combination with seeing estimates. This can be achieved through wind profile and ground layer seeing measurements.

The authors gratefully acknowledge the contribution of R. Robles, NIO, who assisted with data translation. We also thank F. Angeles from the Institute of Astronomy, UNAM, for providing us with the digital topographical data for San Pedro Mártir Sierra.

REFERENCES

Alvarez, M. 1982, Reporte Técnico No. 5, Instituto de Astronomía, UNAM

Alvarez, M., & Maisterrena, J. 1977, RevMexAA, 2, 43

Avila, R., Cruz-González, I., & Tapia, M. 2003, in RevMexAASC, 19, San Pedro Mártir: Astronomical Site Evaluation, eds. I. Cruz-González, R. Avila, & M. Tapis (México City: Inst. Astron., UNAM), 121

Avila, R., Vernin, J., & Cuevas, S. 1998, PASP, 110, 1160

Carrasco, E., & Sarazin, M. 2003, in RevMexAASC, 19, San Pedro Mártir: Astronomical Site Evaluation, eds. I. Cruz-González, R. Avila, & M. Tapis (México City: Inst. Astron., UNAM), 103

Conan, R. et al., 2002, A&A, 396, 723

Davenport, A. G. 1960, Proc. ASCE J. Struct. Div., 86, 39

De Young, D. S., & Charles, R. D. 1995, AJ, 110, 3107

Echevarría et al., 1998, RevMexAA, 34, 47

Erasmus, D. A., & van Staden, C. A. 2002, A Satellite Survey of Cloud Cover and Water Vapor in the Southwestern USA and Northern Mexico. Final Report CELT Project (Pasadena: CALTECH)

Hiriart, D. 2003a, RevMexAA, 39, 119

________. 2003b, in RevMexAASC, 19, San Pedro Mártir: Astronomical Site Evaluation, eds. I. Cruz-González, R. Avila, & M. Tapis (México City: Inst. Astron., UNAM), 90

Hiriart, D., Goldsmith, P. F., Skrutskie, M. F., & Salas, L. 1997, RevMexAA, 33, 59

Hiriart, D., Ochoa, J. L., & García, B. 2001, RevMexAA, 37, 213

Masciadri, E. 2003, RevMexAA, 39, 249

Mendoza, E. E. 1971, Bol. Obs. Tonantzintla y Tacubaya, 6, 95

________. 1973, Mercury, 2, 9

Mendoza, E. E., Luna, J., & Gómez, T. 1972, Bol. Obs. Tonantzintla y Tacubaya, 6, 215

Michel, R., Bohigas, J., Arroyo, E., & Zazueta, S. 2001, RevMexAA, 37,165

Michel, R., Echeverría, J., Costero, R., & Harris, O. 2003, in RevMexAASC, 19, San Pedro Mártir: Astronomical Site Evaluation, eds. I. Cruz-González,

R. Avila, & M. Tapis (México City: Inst. Astron., UNAM), 37
Riemer, M.,& Zangel, G. 2002, Analysis of the Performance of the MM5 for the VLT Site at Paranal, Final Report ESO, contract 66987/ODG/02/6685/GWI/LET, p. 163 (München: Meteorologisches Institut Universität)
Tapia, M. 1997, RevMexAA, 37,165
Walker, M. F. 1971, PASP, 83, 401
__________. 1984, in Site Testing for Future High Telescopes, eds. A. Ardeberg & L. Woljer (Münich: ESO), 3
Wieringa, J. 1996, J. Wind Eng. & Ind. Aerodyn., 65, 1
Westphal, J. A. 1974, Infrared Sky Noise Survey, Final Report NASA-NGR-05-002-185 (Pasadena: CALTECH)

David Hiriart: Instituto de Astronomía, UNAM Campus Ensenada, Apdo. Postal 877, 22830 Ensenada, B. C., México (hiriart@astrosen.unam.mx).
Konstantinos Vogiatzis: AURA-NIO, National Optical Astronomy Observatory, 950 N. Cherry Ave., Tucson, AZ, 85719 USA (voyages@noao.edu).